Hazard Zone Mapping in Respect to the Damages to Wooden Houses due to Breaking of Levee

By Tamotsu TAKAHASHI and Hajime NAKAGAWA

(Mamuscript received March 19, 1987)

Abstract

A numerical simulation method of overland flood flow, in which the effect of buildings and other structures on flow behavior are taken into account is presented to be used in hazard zone mapping in respect to damages to wooden houses. At first, the basic equations and their explicit finite difference expressions are delineated, which assures stable and accurate solutions for overland flood flows. Then a procedure for taking into account the effect of structures on flow behavior is examined. Validity of this simulation method is checked by comparing the results of laboratory model experiments to those obtained through calculations. Subsequently, the criteria for the destruction of wooden houses by a flood flow is discussed. These criteria, combined with the simulation method is used to predict the flood hazardous zones in an actual basin (Ogura basin, situated in the south of Kyoto Prefecture). Finally, we propose a method to estimate the amount of damage by an inundation, and compare the loss calculated under several imaginary bank breach points.

1. Introduction

In Japan, about 50% of its population lives and 70% of owned real estate exist in flood hazardous zones. Although continuous efforts have been devoted to construct flood prevention works, the risks of river bank breach are still very high. In fact, the risks are greater than before due to the progress of the concentration of population and the concomitant structures in hazardous zones. Under these circumstances, 'soft' measures to mitigate disaster are very important. Among various soft measures, which is the modern generic term for non-structural flood prevention measures, the prediction of flood areas and their severity, such as the ranges within which houses would be swept away, or severely inundated, or severely affected by sedimentation etc., would be the most urgent because such predictions would give us an understanding of the degree of safety of life and property. This is the starting point from which to devise strategy against flood hazards.

Our efforts first produced a numerical simulation method of inundation, in which the effect of structures on flow behavior were taken into account. After that, the criteria by which the resistance of wooden structures against being swept away was discussed. This criterion was derived as follows : Wooden houses are comparatively easily swept away due to their weak base structures. Therefore, the criterion of the structural limits beyond which a wooden structure will collapse, is also assumed as the criterion for the limit beyond which a wooden structure would be swept away. The criterion is defined as the condition when the applying moment, M, around the bottom of the

post and beam structures exceeds the maximum resistant moment, M_V. This set of conditions has been derived from a full-scale model test. According to the results of model experiments on hydraulic force acting on the house, there are linear relationships between the moment, M, and the hydraulic force factor u^2A by taking water depth h as a parameter. This relationship is used to draw curves along which critical points are placed. The values of u and h by which these points are plotted will give the criteria for the destruction of post and beam structures by an inundation.

Resistance of window glass against hydrodynamic pressure was also examined and risk of window glass failure which may result in the case of severe damage to the house was discussed employing the same set of coordinates, u and h as in the case of removal by flood.

We tried to predict the flood hazardous zones in an actual basin by combining the simulation method with this criterion corresponding to the several cases of bank breach points. Furthermore, we tried to estimate the amount of loss in each bank breach case by introducing functions to calculate the damage rate of a house under certain combinations of water depth and velocity. These estimations made it possible to discuss various problems such as at which points along a levee would a break cause the most severe damage in the basin, or how does the damage potential change with the change of times, or what would be the effect of closing the breach in the midst of flooding.

2. Basic Equations and Their Finite Difference Scheme for Overland Flood Flows

2.1 Basic Equations

Simplified Reynolds equations can be written as follows :

$$\frac{\partial u}{\partial t}+\frac{\partial (uu)}{\partial x}+\frac{\partial (uv)}{\partial y}+\frac{\partial (uw)}{\partial z}=F_x-\frac{1}{\rho}\frac{\partial p}{\partial x}+\frac{1}{\rho}(\mu+\zeta)\frac{\partial^2 u}{\partial z^2} \quad \cdots\cdots(1)$$

$$\frac{\partial v}{\partial t}+\frac{\partial (vu)}{\partial x}+\frac{\partial (vv)}{\partial y}+\frac{\partial (vw)}{\partial z}=F_y-\frac{1}{\rho}\frac{\partial p}{\partial y}+\frac{1}{\rho}(\mu+\zeta)\frac{\partial^2 v}{\partial z^2} \quad \cdots\cdots(2)$$

$$0=F_z-\frac{1}{\rho}\frac{\partial p}{\partial z} \quad \cdots\cdots(3)$$

The continuity equation is

$$\frac{\partial u}{\partial x}+\frac{\partial v}{\partial y}+\frac{\partial w}{\partial z}=0 \quad \cdots\cdots(4)$$

When we take x, y axes horizontally and z axis vertically, $F_x=F_y=0$, $F_z=-g$, where, $u(t, x, y, z)$, $v(t, x, y, z)$ and $w(t, x, y, z)$ are velocity components in x, y, and z directions, respectively, t=time, g=gravitational force per unit mass, p=pressure, μ=viscosity, ζ=eddy viscosity, ρ=density of fluid. In the case of overland flood flows, flow conditions can be characterized as shallow because the problem possesses much larger horizontal than vertical scales. So that, these equations can be integrated over z direction, under the assumption of hydrostatic pressure distribution, giving the following governing equations :

$$\frac{\partial M}{\partial t}+\frac{\partial}{\partial x}(\beta_{xx}u_0M)+\frac{\partial}{\partial y}(\beta_{xy}v_0M)=-gh\frac{\partial(z_b+h)}{\partial x}-\frac{1}{\rho}\tau_{bx} \quad \cdots\cdots(5)$$

$$\frac{\partial N}{\partial t}+\frac{\partial}{\partial x}(\beta_{yx}u_0N)+\frac{\partial}{\partial y}(\beta_{yy}v_0N)=-gh\frac{\partial(z_b+h)}{\partial y}-\frac{1}{\rho}\tau_{by} \quad \cdots\cdots(6)$$

where, u_0 and v_0 are depth averaged velocity components of x and y directions, respectively, M and N are water discharge per unit width in x and y directions, i. e. $M=u_0h$, $N=v_0h$ we herein call each of them 'flux', h=water depth, z_b=elevation of the base, τ_{bx} and τ_{by} are x and y components of resistance to flow and we assume the following relations.

$$\frac{\tau_{bx}}{\rho}=\frac{gn^2u_0\sqrt{u_0^2+v_0^2}}{h^{1/3}},\quad \frac{\tau_{by}}{\rho}=\frac{gn^2v_0\sqrt{u_0^2+v_0^2}}{h^{1/3}} \quad \cdots\cdots(7)$$

where, n is Manning's roughness coefficient. β_{xx}, β_{xy}, β_{yx}, β_{yy} are momentum correction coefficients, and they are

$$\left.\begin{aligned}\beta_{xx}&=\frac{1}{h}\int_{z_b}^{z_b+h}\left\{1+\left(\frac{u'}{u_0}\right)^2\right\}dz\\ \beta_{xy}&=\frac{1}{h}\int_{z_b}^{z_b+h}\left\{1+\frac{u'v'}{u_0v_0}\right\}dz=\beta_{yx}\\ \beta_{yy}&=\frac{1}{h}\int_{z_b}^{z_b+h}\left\{1+\left(\frac{v'}{v_0}\right)^2\right\}dz,\end{aligned}\right\} \quad \cdots\cdots(8)$$

where u' and v' are fluctuation velocities from u_0 and v_0. In this study, we assumed all these momentum correction coefficients as unity. By integrating eq.(4) from $z=z_b$(bed surfcce) to $z=z_b+h$(water surface) (See **Fig. 1**), we obtain the following continuity equation.

$$\frac{\partial h}{\partial t}+\frac{\partial M}{\partial x}+\frac{\partial N}{\partial y}=0 \quad \cdots\cdots(9)$$

This mathematical model of overland flood flow is restricted only by the aforementioned assumptions and the validity of this model can be extended even to the

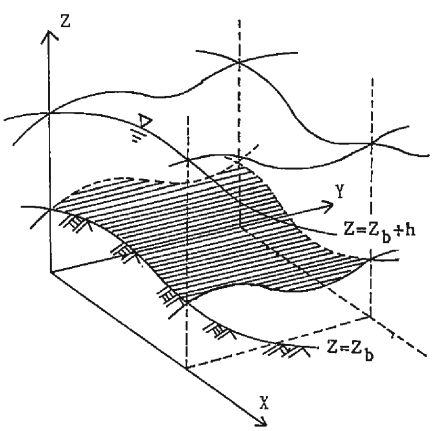

Fig. 1. Definition sketch of coordinates system.

vicinity of the advancing flood front. Furthermore, assuming that the front velocity is equal to the water velocity immediately upstream from the front, this model may be used to represent the whole flow field.

2.2 Finite Difference Scheme

The integration of the system of the equations is achieved numerically. The values to be calculated are the water depth, h, at each mesh center and the fluxes M and N normal to each mesh side. The arrangement of the mesh scheme and the calculation process are shown in **Fig. 2.** The derivatives approximated by finite differences lead finally to the following numerical forms of equations :

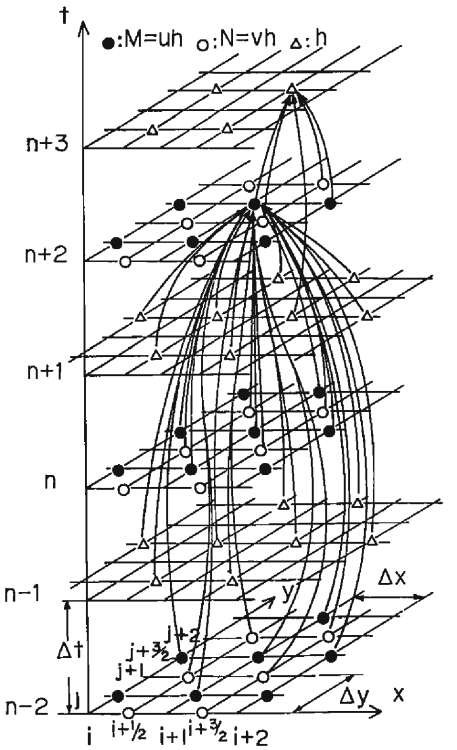

Fig. 2. Grids for two dimensional unsteady flow calculation and arrangement of mesh scheme.

continuity equation

$$\frac{h^{n+3}_{i+1/2,\,j+1/2}-h^{n+1}_{i+1/2,\,j+1/2}}{2\Delta t}+\frac{M^{n+2}_{i+1,\,j+1/2}-M^{n+2}_{i,\,j+1/2}}{\Delta x}+\frac{N^{n+2}_{i+1/2,\,j+1}-N^{n+2}_{i+1/2,\,j}}{\Delta y}=0 \quad \cdots\cdots (10)$$

momentum equation of x-component

$$\frac{M^{n+2}_{i,\,j+1/2}-M^{n}_{i,\,j+1/2}}{2\Delta t}+XDX+XDY$$
$$=-g\frac{(h^{n+1}_{i+1/2,\,j+1/2}+h^{n+1}_{i-1/2,\,j+1/2})\,(h^{n+1}_{i+1/2,\,j+1/2}+z_{bi+1/2,\,j+1/2}-h^{n+1}_{i-1/2,\,j+1/2}-z_{bi-1/2,\,j+1/2})}{2\Delta x}$$

$$-gn^2_{i+1/2,\,j+1/2}\frac{\bar{u}_{i,\,j+1/2}\sqrt{(u^n_{i,\,j+1/2})^2+(v^n_{i,\,j+1/2})^2}}{[(h^{n+1}_{i+1/2,\,j+1/2}+h^{n+1}_{i+1/2,\,j-1/2})/2]^{1/3}} \quad \cdots\cdots(11)$$

momentum equation of y-component

$$\frac{N^{n+2}_{i+1/2,\,j}-N^n_{i+1/2,\,j}}{2\Delta t}+YDX+YDY$$
$$=-g\frac{(h^{n+1}_{i+1/2,\,j+1/2}+h^{n+1}_{i+1/2,\,j-1/2})\,(h^{n+1}_{i+1/2,\,j+1/2}+z_{bi+1/2,\,j+1/2}-h^{n+1}_{i+1/2,\,j-1/2}-z_{bi+1/2,\,j-1/2})}{2\Delta y}$$
$$-gn^2_{i+1/2,\,j+1/2}\frac{\bar{v}_{i+1/2,\,j}\sqrt{(u^n_{i+1/2,\,j})^2+(v^n_{i+1/2,\,j})^2}}{[(h^{n+1}_{i+1/2,\,j+1/2}+h^{n+1}_{i+1/2,\,j-1/2})/2]^{1/3}} \quad \cdots\cdots(12)$$

where

$$\bar{u}_{i,\,j+1/2}=\frac{M^{n+2}_{i,\,j+1/2}+M^n_{i,\,j+1/2}}{h^{n+1}_{i+1/2,\,j+1/2}+h^{n+1}_{i-1/2,\,j+1/2}} \quad \cdots\cdots(13a)$$

$$\bar{v}_{i+1/2,\,j}=\frac{N^{n+2}_{i+1/2,\,j}+N^n_{i+1/2,\,j}}{h^{n+1}_{i+1/2,\,j+1/2}+h^{n+1}_{i+1/2,\,j-1/2}} \quad \cdots\cdots(13b)$$

$$u^n_{i,\,j+1/2}=\frac{2(M^n_{i,\,j+1/2}+M^{n-2}_{i,\,j+1/2})}{h^{n+1}_{i+1/2,\,j+1/2}+h^{n+1}_{i-1/2,\,j+1/2}+h^{n-1}_{i+1/2,\,j+1/2}+h^{n-1}_{i-1/2,\,j+1/2}} \quad \cdots\cdots(14a)$$

$$u^n_{i+1/2,\,j}=\frac{1}{4}\Bigg[\frac{2(M^n_{i+1,\,j+1/2}+M^{n-2}_{i+1,\,j+1/2})}{h^{n+1}_{i+3/2,\,j+1/2}+h^{n+1}_{i+1/2,\,j+1/2}+h^{n-1}_{i+3/2,\,j+1/2}+h^{n-1}_{i+1/2,\,j+1/2}}$$
$$+\frac{2(M^n_{i,\,j+1/2}+M^{n-2}_{i,\,j+1/2})}{h^{n+1}_{i+1/2,\,j+1/2}+h^{n+1}_{i-1/2,\,j+1/2}+h^{n-1}_{i+1/2,\,j+1/2}+h^{n-1}_{i-1/2,\,j+1/2}}$$
$$+\frac{2(M^n_{i+1,\,j-1/2}+M^{n-2}_{i+1,\,j-1/2})}{h^{n+1}_{i+3/2,\,j-1/2}+h^{n+1}_{i+1/2,\,j-1/2}+h^{n-1}_{i+3/2,\,j-1/2}+h^{n-1}_{i+1/2,\,j-1/2}}$$
$$+\frac{2(M^n_{i,\,j-1/2}+M^{n-2}_{i,\,j-1/2})}{h^{n+1}_{i+1/2,\,j-1/2}+h^{n+1}_{i-1/2,\,j-1/2}+h^{n-1}_{i+1/2,\,j-1/2}+h^{n-1}_{i-1/2,\,j-1/2}}\Bigg] \quad \cdots\cdots(14b)$$

$$v^n_{i,\,j+1/2}=\frac{1}{4}\Bigg[\frac{2(N^n_{i+1/2,\,j+1}+N^{n-2}_{i+1/2,\,j+1})}{h^{n+1}_{i+1/2,\,j+3/2}+h^{n+1}_{i+1/2,\,j+1/2}+h^{n-1}_{i+1/2,\,j+3/2}+h^{n-1}_{i+1/2,\,j+1/2}}$$
$$+\frac{2(N^n_{i+1/2,\,j+1}+N^{n-2}_{i+1/2,\,jn+1})}{h^{n+1}_{i+1/2,\,j+1/2}+h^{n+1}_{i+1/2,\,j-1/2}+h^{n-1}_{i+1/2,\,j+1/2}+h^{n-1}_{i+1/2,\,j-1/2}}$$
$$+\frac{2(N^n_{i-1/2,\,j+1}+N^{n-2}_{i-1/2,\,j+1})}{h^{n+1}_{i-1/2,\,j+3/2}+h^{n+1}_{i-1/2,\,j+1/2}+h^{n-1}_{i-1/2,\,j+3/2}+h^{n-1}_{i-1/2,\,j+1/2}}$$
$$+\frac{2(N^n_{i-1/2,\,j}+N^{n-2}_{i-1/2,\,j})}{h^{n+1}_{i-1/2,\,j+1/2}+h^{n+1}_{i-1/2,\,j-1/2}+h^{n-1}_{i-1/2,\,j+1/2}+h^{n-1}_{i-1/2,\,j-1/2}}\Bigg] \quad \cdots\cdots(15a)$$

$$v^n_{i+1/2,\,j}=\frac{2(N^n_{i+1/2,\,j}+N^{n-2}_{i+1/2,\,j})}{h^{n+1}_{i+1/2,\,j+1/2}+h^{n+1}_{i+1/2,\,j-1/2}+h^{n-1}_{i+1/2,\,j+1/2}+h^{n-1}_{i+1/2,\,j-1/2}} \quad \cdots\cdots(15b)$$

XDX, *XDY*, *YDX* and *YDY* are non-linear convection terms, in order to save space,

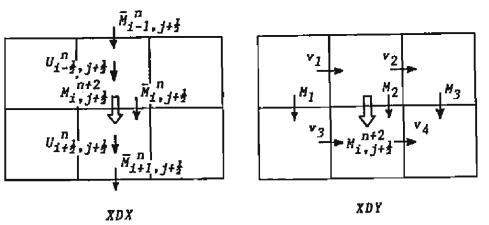

Fig. 3. Arrangement of u_0, v_0 and M in calculation of *XDX* and *XDY*.

only the finite difference expressions of XDX and XDY terms are presented below[1] (See **Fig. 3**) :

$$\left.\begin{aligned} XDX &= (U^n_{i+1/2,j+1/2}\bar{M}^n_{i,j+1/2} - U^n_{i-1/2,j+1/2}\bar{M}^n_{i-1,j+1/2})/\Delta x, \\ &\qquad (U^n_{i+1/2,j+1/2}\geq 0,\ U^n_{i-1/2,j+1/2}\geq 0) \\ &= (U^n_{i+1/2,j+1/2}\bar{M}^n_{i,j+1/2} - U^n_{i-1/2,j+1/2}\bar{M}^n_{i,j+1/2})/\Delta x, \\ &\qquad (U^n_{i+1/2,j+1/2}\geq 0,\ U^n_{i-1/2,j+1/2}< 0) \\ &= (U^n_{i+1/2,j+1/2}\bar{M}^n_{i+1,j+1/2} - U^n_{i-1/2,j+1/2}\bar{M}^n_{i-1,j+1/2})/\Delta x, \\ &\qquad (U^n_{i+1/2,j+1/2}< 0,\ U^n_{i-1/2,j+1/2}\geq 0) \\ &= (U^n_{i+1/2,j+1/2}\bar{M}^n_{i+1/2,j+1/2} - U^n_{i-1/2,j+1/2}\bar{M}^n_{i,j+1/2})/\Delta x, \\ &\qquad (U^n_{i+1/2,j+1/2}< 0,\ U^n_{i-1/2,j+1/2}< 0) \end{aligned}\right\} \cdots\cdots (16a)$$

$$XDY = \{(v_0M)_f - (v_0M)_b\}/\Delta y \cdots\cdots (16b)$$

where

$$U^n_{i+1/2,j+1/2} = \frac{M^n_{i+1,j+1/2} + M^{n-2}_{i+1,j+1/2}}{h^{n+1}_{i+3/2,j+1/2} + h^{n+1}_{i+1/2,j+1/2} + h^{n-1}_{i+3/2,j+1/2} + h^{n-1}_{i+1/2,j+1/2}} + \frac{M^n_{i,j+1/2} + M^{n-2}_{i,j+1/2}}{h^{n+1}_{i+1/2,j+1/2} + h^{n+1}_{i-1/2,j+1/2} + h^{n-1}_{i+1/2,j+1/2} + h^{n-1}_{i-1/2,j+1/2}} \cdots\cdots (17)$$

$$\bar{M}^n_{i,j+1/2} = \frac{M^n_{i,j+1/2} + M^{n-2}_{i,j+1/2}}{2} \cdots\cdots (18)$$

$$M_1 = \bar{M}^n_{i-1,j+1/2},\quad M_2 = \bar{M}^n_{i,j+1/2},\quad M_3 = \bar{M}^n_{i+1,j+1/2} \cdots\cdots (19)$$

$$\left.\begin{aligned} v_1 &= \frac{2(N^n_{i-1/2,j} + N^{n-2}_{i-1/2,j})}{h^{n+1}_{i-1/2,j+1/2} + h^{n+1}_{i-1/2,j-1/2} + h^{n-1}_{i-1/2,j+1/2} + h^{n-1}_{i-1/2,j-1/2}} \\ v_2 &= \frac{2(N^n_{i-1/2,j+1} + N^{n-2}_{i-1/2,j+1})}{h^{n+1}_{i-1/2,j+3/2} + h^{n+1}_{i-1/2,j+1/2} + h^{n-1}_{i-1/2,j+3/2} + h^{n-1}_{i-1/2,j+1/2}} \\ v_3 &= \frac{2(N^n_{i+1/2,j} + N^{n-2}_{i+1/2,j})}{h^{n+1}_{i+1/2,j+1/2} + h^{n+1}_{i+1/2,j-1/2} + h^{n-1}_{i+1/2,j+1/2} + h^{n-1}_{i+1/2,j-1/2}} \\ v_4 &= \frac{2(N^n_{i+1/2,j+1} + N^{n-2}_{i+1/2,j+1})}{h^{n+1}_{i+1/2,j+3/2} + h^{n+1}_{i+1/2,j+1/2} + h^{n-1}_{i+1/2,j+3/2} + h^{n-1}_{i+1/2,j+1/2}} \end{aligned}\right\} \cdots\cdots (20)$$

$$\left.\begin{aligned} (v_0M)_f &= (v_4M_2 + v_2M_3)/2, && (v_4\geq 0,\ v_2< 0,\ M_2\geq 0,\ M_3< 0) \\ &= (v_4M_3 + v_2M_2)/2, && (v_4< 0,\ v_2\geq 0,\ M_2< 0,\ M_3\geq 0) \\ &= v_4M_2, && (v_4\geq 0,\ v_2< 0,\ M_2\geq 0,\ M_3\geq 0 \\ &&& \quad \text{or } v_4\geq 0,\ v_2\geq 0,\ M_2\geq 0) \\ &= v_4M_3, && (v_4< 0,\ v_2\geq 0,\ M_2\geq 0,\ M_3\geq 0 \\ &&& \quad \text{or } v_4< 0,\ v_2< 0,\ M_3\geq 0) \\ &= v_2M_3, && (v_4\geq 0,\ v_2< 0,\ M_2< 0,\ M_3< 0 \\ &&& \quad \text{or } v_4< 0,\ v_2< 0,\ M_3< 0) \\ &= v_2M_2, && (v_4< 0,\ v_2\geq 0,\ M_2< 0,\ M_3< 0 \\ &&& \quad \text{or } v_4\geq 0,\ v_2\geq 0,\ M_2< 0) \\ &= 0, && (\text{the others}) \end{aligned}\right\} \cdots\cdots (21)$$

$$\left.\begin{aligned} (v_0M)_b &= (v_3M_1 + v_1M_2)/2, && (v_3\geq 0,\ v_1< 0,\ M_1\geq 0,\ M_2< 0) \\ &= (v_3M_2 + v_1M_1)/2, && (v_3< 0,\ v_1\geq 0,\ M_1< 0,\ M_2\geq 0) \\ &= v_3M_1, && (v_3\geq 0,\ v_1< 0,\ M_1\geq 0,\ M_2\geq 0 \\ &&& \quad \text{or } v_3\geq 0,\ v_1\geqq 0,\ M_1\geq 0) \end{aligned}\right\}$$

$$
\left.\begin{aligned}
&=v_3M_2 && , (v_3<0,\ v_1\geq 0,\ M_1\geq 0,\ M_2\geq 0\\
& && \quad \text{or } v_3<0,\ v_1<0,\ M_2\geq 0)\\
&=v_1M_2 && , (v_3\geq 0,\ v_1<0,\ M_1<0,\ M_2<0\\
& && \quad \text{or } v_3<0,\ v_1<0,\ M_2<0)\\
&=v_1M_1 && , (v_3<0,\ v_1\geq 0,\ M_1<0,\ M_2<0\\
& && \quad \text{or } v_3>0,\ v_1\geq 0,\ M_1<0)\\
&=0 && , (\text{the others})
\end{aligned}\right\} \quad \cdots\cdots\cdots (22)
$$

Unknowns in these equations are M^{n+2}, N^{n+2} and h^{n+3}, so that, except at the boundary, we can obtain values for M^{n+2} and N^{n+2} by substituting the known M^n, N^n and h^{n+1} values into eq.(11) and eq.(12). Next, substituting these values into eq. (10), we obtain the values of h^{n+3}. Calculation of the inertia terms by the finite difference approximation is accomplished by using h^{n-1}, M^{n-2} and N^{n-2} as was introduced by Iwasa and Inoue[2].

The boundary condition at the fixed plain boundaries is that the mean velocity normal to the boundary is zero. The flood front of the flow is a moving boundary and presents a difficult problem even for computer-aided analysis. The present analysis sacrifices strictness of mass conservation to some extent to get rid of the complexity at the forefront. The alternative simplified treatment is that if the computation yields a flow depth less than a certain small threshold value in a mesh, the forefront is regarded as not having arrived yet, so that no flux is generated from this mesh.

2.3 Consideration of the Effect of the Existence of Structures in a Mesh

As the overland flood flows are affected by the existence of houses and other structures, we must consider this effect. So far, two dimensional overland flood flows have been simulated by giving a certain roughness coefficient or equivalent friction coefficient respectively to the urban area, agricultural land, forest and so forth. For example, Xanthopoulos et al[3]. adopted Manning's roughness coefficient $n=0.067$ for the village, 0.025 for the cultivated area, 0.040 and 0.033 for the tree area and bush areas, respectively. Aida[4] obtained an equivalent friction coefficient f_e by considering the energy loss due to the screening effects of the buildings on the run-up of a tsunami, and he used $f_e=0.1$ for the structure dense area. By comparing the results of numerical simulation with experimental results, Nakagawa et al[5]. proved that if the proper value of roughness coefficient is chosen in each mesh corresponding to the density of real estate development in it, it was possible to simulate the behavior of the overland flood flows in the fleld quite accurately. But it is very difficult to evaluate the roughness coefficient based on the greatly varying density of structures from area to area. Goto et al[6]. proposed the following equivalent roughness coefficient:

$$
n_e=\frac{h^{4/3}}{2gl_1}\left(\frac{1}{c_e^2}-1\right) \quad \cdots\cdots\cdots (23)
$$

where, n_e=equivalent roughness coefficient, l_1=distance from the front row of a group of buildings to the range where the energy loss is evident by the contraction of flow, c_e=discharge coefficient presented by the function of Froude number and the contraction

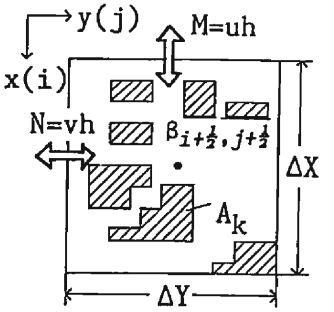

Fig. 4. Definition sketch for evaluating the effects of houses in a mesh to the behavior of the flooding water.

coefficient. In this equation, there is a problem how to decide the value l_1. The information we can obtain from the topographical maps, are the number of buildings, total area of structures, arrangement of structures and so forth. But it might be very difficult to consider all this information into calculations for equivalent roughness. Hence, alternative to estimating the equivalent roughness coefficient, a method is presented that uses the concept of flux correction factor. This factor, β, is defined as the rate of area occupied by structures to a mesh area($\Delta x \Delta y$), namely, β is calculated at each mesh center $(i+1/2, j+1/2)$ (See **Fig. 4**):

$$\beta_{i+1/2,j+1/2}=\sqrt{1-\sum_k A_k/\Delta x\Delta y} \quad \cdots\cdots(24)$$

where, $\sum_k A_k$=total area occupied by the structures. In this treatment, it is assumed that the scale of a mesh is sufficiently larger than the area occupid by any structure and that the structures in a mesh are scattered widely. Fluxes M and N are modified as follows:

$$\tilde{M}^{n+2}_{i,j+1/2}=\beta_{a,j+1/2}M^{n+2}_{i,j+1/2}\begin{cases}M^{n+2}_{i,j+1/2}\geqq 0 : a=i+1/2\\ M^{n+2}_{i,j+1/2}<0 : a=i-1/2\end{cases} \quad \cdots\cdots(25)$$

$$\tilde{N}^{n+2}_{i+1/2,j}=\beta_{i+1/2,b}N^{n+2}_{i+1/2,j}\begin{cases}N^{n+2}_{i+1/2,i}\geqq 0 : b=j+1/2\\ N^{n+2}_{i+1/2,i}<0 : b=j-1/2\end{cases} \quad \cdots\cdots(26)$$

By substituting eq.(25) and eq. (26) into eq.(10), we obtain the modified water depth:

$$\tilde{h}^{n+3}_{i+1/2,j+1/2}=\tilde{h}^{n+1}_{i+1/2,j+1/2}-\frac{2\Delta t}{\Delta x}(\tilde{M}^{n+2}_{i+1,j+1/2}-\tilde{M}^{n+2}_{i,j+1/2})-\frac{2\Delta t}{\Delta y}(\tilde{N}^{n+2}_{i+1/2,j+1}-\tilde{N}^{n+2}_{i+1/2,j}) \quad \cdots\cdots(27)$$

3. Comparison with Laboratory Experiment

A quantitative test of the numerical model was done by comparing the results with the experimental outcomes. A situation is simulated, where the river bank is partially destroyed within an extremely short time interval and the two dimensional flood propagates over a horizontal dry bed surface.

3.1 Experimental Set-up

The experimental set-up is shown in **Fig. 5.** The flood plain area is 1.84m×1.84m and the bank breach is 20 cm wide. Urethane blocks, 2.5 cm wide, 2.5 cm long and 3.0 cm high, were arranged on the dry bed, and simulate the group of structures. A flooding was generated by pulling the gate up in an instant.

The surface velocity and the depth of flow at the breach point were measured by a high-speed TV-video camera and a servo-type water level gauge, respectively. The expanding shape of the flood front was measured by an another video camera. Water depth along the flow axis perpendicular to the breach at the distance of 0 cm, 50 cm, 100 cm and 150 cm from the breach point was measured with 4 channel servo-type water level gauges. Sampling speed was 125 Hz and the data were monitored on the pen-recorder and recorded into a data recorder.

Hydrograph and water depth at the breach point are shown in **Fig. 6.** Concerning the water discharge, since it was evaluated by using water surface velocity and water depth at the breach point, the value may be slightly larger than the actual water discharge. Experimental conditions are shown in **Table 1,** where B_0=width of the bank breach, H_0=initial water depth in the tank shown in **Fig. 5,** i=bed slope, n=Manning's roughness coefficient ($m^{-1/3}sec$), B=distance from block to block. For the CASE-1, there are no blocks on the bed. The flow freely descends to the downstream end of the flood plain.

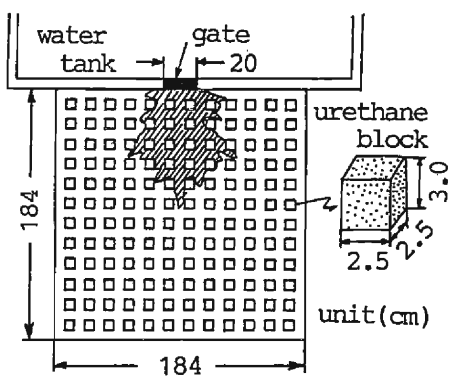

Fig. 5. Experimental setup.

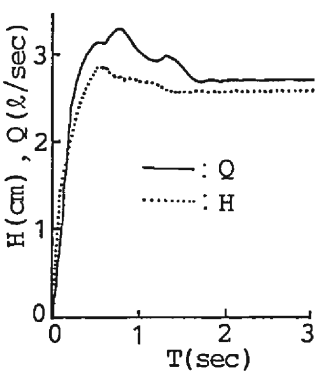

Fig. 6. Hydrograph and water depth at bank breach point.

Table 1. Experimental conditions of the floodings due to sudden bank breach.

	CASE	B(cm)
B_0=20cm H_0= 5cm i=0 n=0.01	1	
	2	2.5
	3	5.5
	4	10.5

3.2 Results and Discussion

Conditions of calculation are shown in **Table 2,** where, Δt=split time of calculation. In CASE-3 and CASE-4, $\beta_{i+1/2,j+1/2}=0.87(=\sqrt{1-0.25})$ as $\Delta x=\Delta y=5$ cm and $\sum_k A_k=6.25$ cm^2. In CASE-2, $\Delta x=\Delta y=2.5$ cm, which is equal in size to one block. Thus, in this case, in one mesh there is no block and in the other mesh the mesh area is wholly occupied by a block. In this case, β is either 0 or 1.

Table 2. Conditions of calculation for the floodings due to sudden bank breach.

	CASE	B(cm)	Δx(cm)	Δy(cm)
$B_0=20$cm $H_0=5$cm $i=0$ $\Delta t=0.001$ (sec)	1		4.0	4.0
	2	2.5	2.5	2.5
	3	5.0	5.0	5.0
	4	10.0	5.0	5.0

The shapes of flood front and surface profiles along the flow axis at $t=1$, 2, and 3 seconds after the bank breach are shown in **Fig. 7.** In CASE-1, although the calculated shapes of the flood front show a little greater expansion than the experimental ones, they are in comparatively good agreement. Therefore, we can regard this simulation model as appropriate under the condition of the uniform dry bed surface. In CASE-2, the calculated results are in very good agreement with the experimental ones, but this scheme requires much process time for computation because the values for Δx, Δy and Δt are very small. Considering the application of the method to the actual basin, it may be impossible to take each structure into account and to use such small scale Δx or Δy. In CASE-3 and CASE-4, we used values twice as large for Δx and Δy, and considered the effects of the blocks by introducing the correction coefficient $\beta_{i+1/2,j+1/2}$. Both calculated shapes of flood front and the water surface profiles along the flow axis are comparatively in good agreement with the experimental ones except for those occassions when the flood fronts are advancing diagonally among the blocks in CASE-4. From these results, we obtained satisfactory descriptive properties of the model for the each case, and the validity of this model was verified from the actual experimental results.

4. Criterion for the Destruction of Wooden Houses by a Flood Flow

Some investigations[4),7)] have found the empirical relationship between hydrodynamic force and the destruction or removal of wooden houses due to a flood flow, but they have not considered the mechanism of destruction itself. Here, we focus on finding the critical condition for removal of the wooden houses by discussing the hydrodynamic force applying to the structures and the resisting mechanism to this force.

The base structure of a typical contemporary Japanese-style wooden house is shown

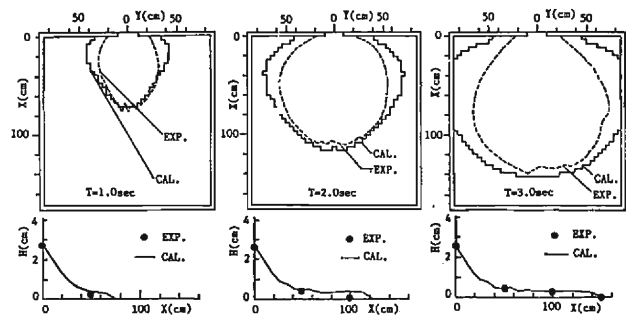

(a) CASE-1

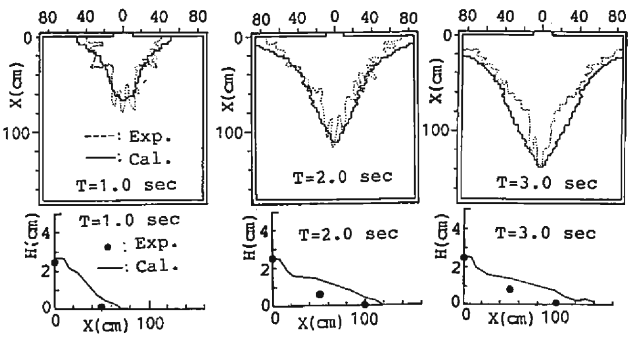

(b) CASE-2

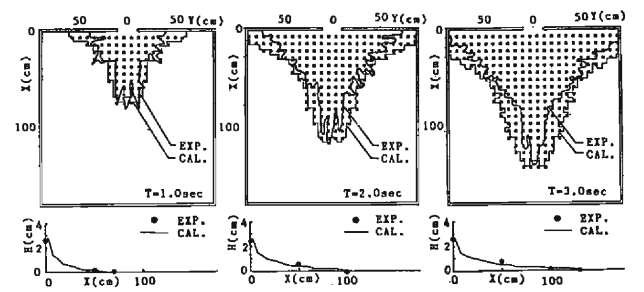

(c) CASE-3

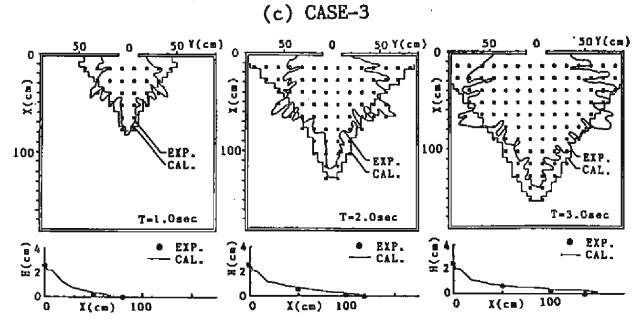

(d) CASE-4

Fig. 7. Comparison between experimental results with calculated ones concerned with shapes of flooding and water surface profiles along the flow axis.

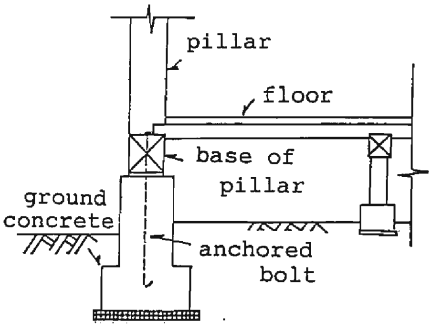

Fig. 8. Example of base structure of typical contemporary Japanese-style wooden house.

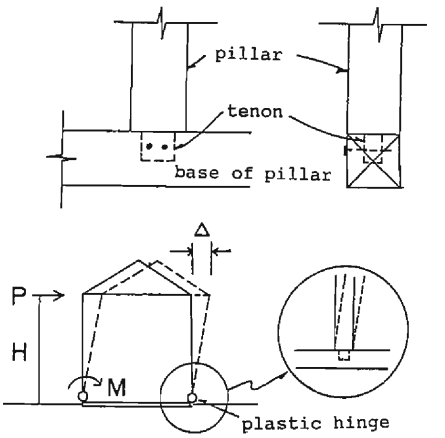

Fig. 9. Behavior of tenon as plastic hinge subject to lateral load.

in **Fig. 8.** The base of post and beam structure is rather strongly bound with anchor bolts. However, the joint where the beam forms a crosspiece is tenon structure. As shown in **Fig. 9,** this joint behaves as a plastic hinge resisting a moment caused by a lateral load such as the hydrodynamic force of a flow and therefore, this may be the most weak point of the whole structure. We presume the dislodgement and removal of a wooden house in floodings occurs primarily by the destruction of this point, while the common believe that buoyant force acts as an important foctor may also be true to some extent. Since the effect of flooding on tenon jointing has yet to be investigated it is hoped that future research on this point will be undertaken.

4.1 Laboratory Experiments

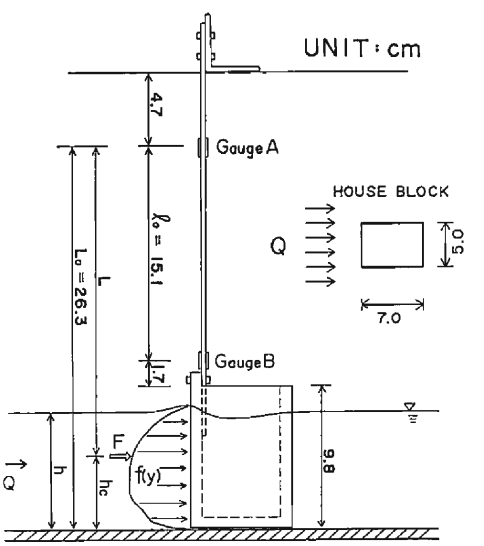

Fig. 10. Profile of experimental model house.

The experimental flume (50 cm wide, 20 cm deep and 5 m long) and a structure model are shown in **Fig. 10.** This model structure (5.0 cm wide, 7.0 cm long and 9.8 cm high) hung by a stiff brass plate was set in the flow, and the drag force (or 'hydrodynamic' force) was measured. The measurement of the force was accomplished by using 4 pieces of strain gauge attached to both sides of the brass plate and by the following equation :

$$F=EI(\varepsilon_A-\varepsilon_B)/el_0 \quad \cdots\cdots(28)$$

where, ε_A and ε_B=change in length due to strain A and B, respectively, E=Young's modulus of plate, I=geometrical moment of inertia, e=edge distance, l_0=distance from A gauge to B, and the value of EI/el_0 is constant($=1.94859\times10^9$ dyn) in this experiment. The height of the acting point of the force, h_c, is obtained by :

$$h_c=L_0-\varepsilon_A l_0(\varepsilon_A-\varepsilon_B) \quad \cdots\cdots(29)$$

where, L_0 is a distance from A gauge to the bottom of the flume.

Experimental conditions are shown in **Table 3.** We show the relationship between hydrodynamic force F and the factor u^2A in **Fig. 11,** in which $A=Bh$ and B is the width of the model structure. From this figure, the following relationship was obtained:

Table 3. Experimental conditions for demonstrating the hydrodynamic force acting on the house model.

Q(cm³/s)	R_e	h(cm)	u(cm/s)	F_r
4079	6230	4.56—9.48	8.61—17.89	0.089—0.268
4992	8330	4.95—9.24	10.81—20.17	0.114—0.290
6166	10230	5.36—9.26	13.32—23.01	0.240—0.317
7157	11760	5.66—9.32	15.36—25.29	0.161—0.340
8174	12480	6.01—9.45	17.30—27.20	0.180—0.354
9179	14010	6.31—9.32	19.70—29.09	0.206—0.370

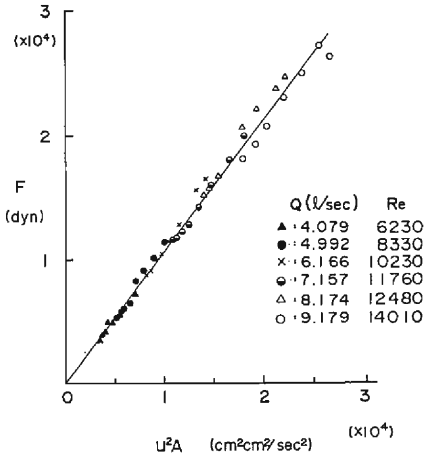

Fig. 11. Relationship between drag force F and hydraulic force factor u^2A.

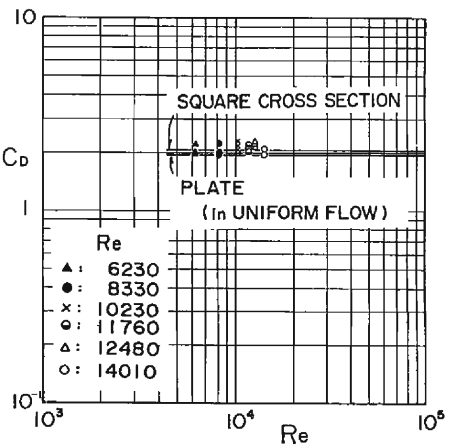

Fig. 12. Relationship between drag coefficient and Reynolds number.

$$\frac{F}{\rho u^2 A}=1.064 \quad \cdots\cdots(30)$$

The relationship between drag coefficient and Reynolds number obtained from these experiments are shown in **Fig. 12.** The variation of the drag coefficient to the Reynolds number is rather slight. This is because the points at which the stream of water separates from a square structure model with sharp edges do not change as in the case of a cylinder. Furthermore, the wakes generated for the square cross sectional body shape having sharp edges like this house model are stable. In this experimental range (Froude number 0.089-0.370, Reynolds number 6230-14010), the drag coefficients in the open channel shear flow takes similar values in the uniform flow.

The height of point of action obtained from eq. (29) is shown in **Fig. 13.** The ensemble mean value of h_c/h was 0.732.

If the approaching velocity profile is approximated according to the following logarithmic law :

$$u/u_*=5.5+5.75\log(u_* y/\nu),\ (\delta<y<h) \quad \cdots\cdots(31)$$

the drag force, R, and moment, M, are obtained under the assumption that the drag coefficient C_D is constant :

$$R=\frac{1}{2}\rho C_D B h u_*^2\left[\{9.025Re_*)\}^2-2ln(9.025Re_*)+2\right]/\kappa^2 \quad \cdots\cdots(32)$$

$$M=\frac{1}{2}\rho C_D B h^2 u_*^2\left[\{ln(9.025Re_*)\}^2-\frac{1}{2}ln(9.025Re_*)+\frac{1}{4}\right]/\kappa^2 \quad \cdots\cdots(33)$$

where, $u_*=\sqrt{gIh}$, I=channel slope (1/3600), $Re_*=u_*h/\nu$, ν=kinematic viscosity and κ= Kármán constant. Eq.(32) and (33) yield the following relationship :

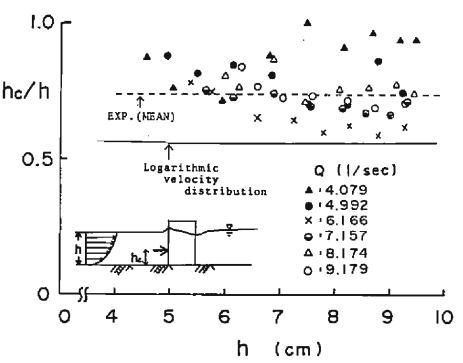

Fig. 13. Experimental and theoretical data concerned with the height and the acting point by the hydrodynamic force.

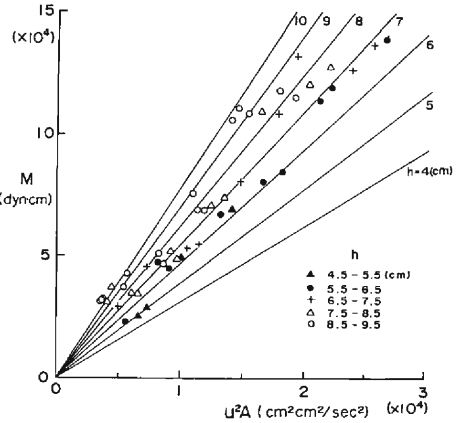

Fig. 14. Relationship between u^2A and moment M taking depth h as a parameter in hydraulic experiments.

$$h_c=\frac{M}{R}=\frac{0.5\{ln(9.025Re_*-0.5\}^2+1/8}{\{ln(9.025Re_*)-1\}^2+1}h \quad \cdots\cdots(34)$$

This relation is also shown in **Fig. 13.** Within the limits of experimental Re_*, h_c/h assumes a nearly constant value of 0.55, independent of the water depth, which is smaller than the experimental ones. The reason may be that in the analysis we didn't consider the effects of rising and falling of the water level in front and behind the model structure. Therefore, in the following analysis, we adopted the experimental value for h_c/h.

The relationships between u^2A and M are shown in **Fig. 14.** The value of M in the experiments is evaluated by using eqs. (28) and (29). The straight lines in this figure were evaluated by

$$M=h_cF=0.732hF=0.779u^2A \quad \cdots\cdots(35)$$

taking water depth, h, as a parameter. From this figure, it was found that there were linear relationships between M around the bottom of the pillar and the hydrodynamic force factor u^2h. These relationships in the prototype scale are shown in **Fig. 15** after carrying out Froude similarity transformation. Geometric similarity scale was taken as $L_m/L_p=\lambda=1/109$[8], where L_m is a model house scale and L_p is a prototype house scale. Here, we used the scale of a typical Japanese wooden house for L_m, which was used for the bearing force test described as follows. Bearing momental values of the full scale Japanese-style wooden house are also shown in this figure for each structural element. In **Table 4,** examples of bearing capacity of the wooden house are shown, which were obtained by a full-scale test on a typical Japanese wooden house subject to cyclic static lateral load[9]. In this table TYPE-I has a basic frame structure composed of only post and beam structures, beams, floors and a roof. TYPE-II and IV have, in addition to the basic frame structure, different types of diagonal beams. In TYPE-III,

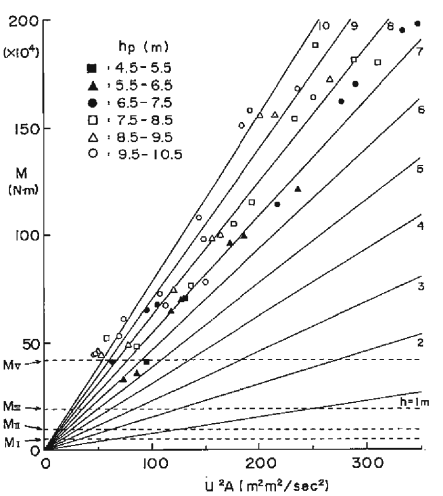

Fig. 15. Relationship between u^2A and M taking water depth h as a barameter after similarity transformation. Bearing moments of the full scale Japanese house are shown for the each structural elements.

Table 4. Example of bearing capacity of the typical Japanese wooden house.

TYPE	F	M	h_e
I	0.95	49110	5.275
II	1.86	96153	5.275
III	3.70	191272	5.275
IV	1.95	100805	5.275
V	8.10	418730	5.275

F : Total bearing capacity (ton)
M : Total bearing moment (Nm)
h_e : Height of action point (m)

plywood walls are added to TYPE-I. TYPE-V is a complete wooden house. In **Fig. 15,** $M_{\rm I}$, $M_{\rm II}$, ···correspond to the bearing moments of TYPE-I, II, ···. The bearing capacity of the full scale house is, therefore, assumed to be equal to that of TYPE-V.

By taking the bearing moment for the full scale Japanese-style wooden house as M_V, we obtained the following critical combinations of depth and velocity of the flood flow which would theoretically destroy the houses :

$$uh \geq \sqrt{M_V/(h_c/h \cdot C_D/2 \cdot \rho)}/\sqrt{B} \quad \cdots\cdots (36)$$

The curves in **Fig. 16** show this relationship for the case $B=5$, 7 and 10 m, respectively by using the values of $M_V=418730$Nm, $C_D/2=1.064$, $h_c/h=0.732$, $\rho=1000$ kg/m^3. The upper range of each curve is the danger zones wherein a wooden house might be swept away. In this figure, three symbols are plotted. Open and full circles

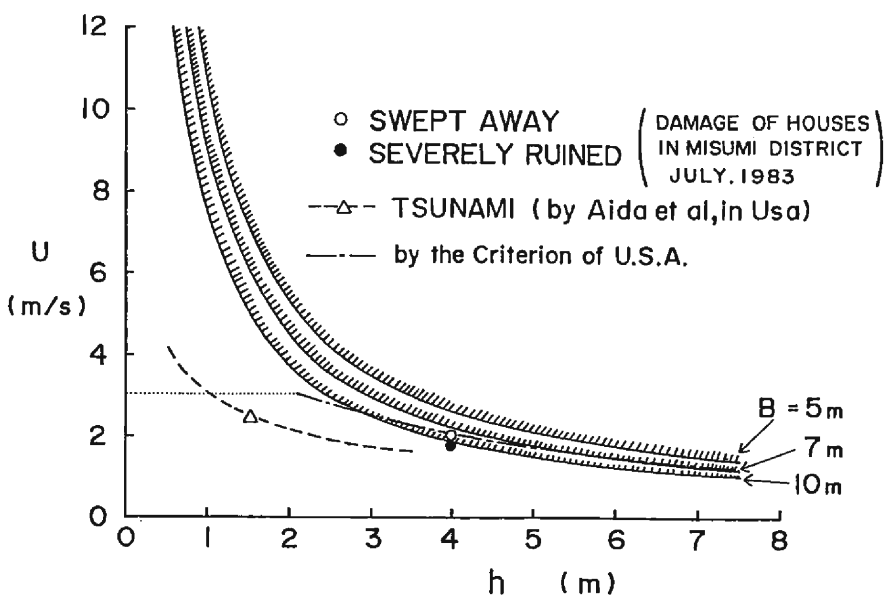

Fig. 16. Critical lines concerned with the house destruction.

are the data presented by Kawata and Nakagawa[7], each, respectively corresponds to washed away and severely ruined houses, which were obtained by a calculation of overland flood flow and a field survey of the Misumi district after a heavy rainfall on 7/23 in 1983. The triangle is the data presented by Aida[4] which was obtained by a method similar to the case of the tsunami disaster in the Usa district, Kochi prefecture due to the Nankai earthquake in 1946. In **Fig. 16,** river flooding data shows rather good agreement with the critical lines, whereas, the tsunami datum does not. The main reason for this discrepancy is presumably attributable to the difference in the mechanism of the external force between flow and wave, namely, the aspect of the flooding in Misumi district is similar to that of the experiment, while the behavior of tsunami flooding is wavy similar to surf and backwash. Therefore, there may be limitations to relating only the hydrodynamic force of tsunami floodings with destruction of a wooden house. As these data depend on the accuracy of the calculations for the base structures and the width of a wooden house, it is necessary to examine the applicability of these criteria by collecting more actual data.

4.2 Criterion for the Breaking of Window Glass

Partial destruction of houses should also be considered in a flooding, such as the phenomena associated with the breaking of window glass. Ishizaki[10] proposed an equation for the allowable wind pressure on a glass window :

$$P_a(T)=fS\frac{t_g}{a}\left(1+K\frac{t_g}{b}\log\frac{10^m}{T}\right) \quad \cdots\cdots(37)$$

where, P_a=allowable wind pressure, T=duration of loading, a, b=short and long sides of glass, respectively, S, K and m=constants and $S=3.5\times10^4\sim5.0\times10^4$ kgf/m^2, $K=70$ and $m=7$, f=strength factor, t_g=thickness of glass plate. The wind pressure effects on the window glass per unit area is :

$$P=\frac{1}{2}\rho u^2C \quad \cdots\cdots(38)$$

where, ρ=density of air (kg · sec^2/m^4), u=wind velocity(m/sec), C=wind pressure factor. When applying this equation to hydraulic pressure, we assumed that the distribution of hydrodynamic force is uniform. However hydrostatic pressure is neglected for

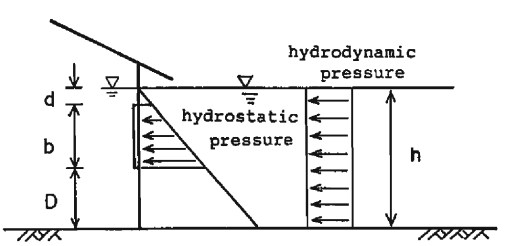

D:elevation of lower frame
d:depth from upper frame to water surface
b:length of window
h:water depth

Fig. 17. Model of flow field against hydraulic pressure.

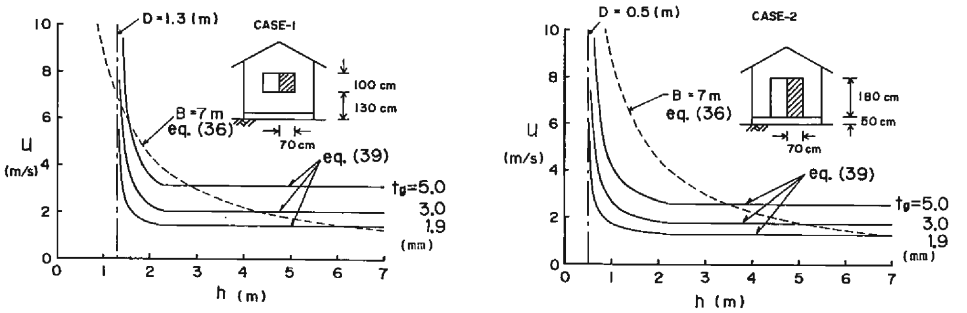

Fig. 18. Critical lines concerned with the window glass.

Table 5. Conditions for the calculation of the criteria for occurrence of window glass breakage.

	a(m)	b(m)	D(m)	t_g(mm)
CASE-1	0.7	1.0	1.3	1.9, 3.0, 5.0
CASE-2	0.7	1.8	0.5	1.9, 3.0, 5.0

$f=0.5$, $S=4\times10^4$, $T=1.0$, $K=70$, $m=7$

the reason that the house is considered as already submerged, so that the water level inside the house is equal to that outside, as shown in **Fig. 17.** From eqs. (37) and (38), the relationship between the flow depth h and the velocity u which will present the allowable bearing capacity of the window glass is derived as follows :

$$u=\sqrt{\frac{2}{\rho C}fS\frac{t_g}{a}\left(1+K\frac{t_g}{h-D}\log\frac{10^m}{T}\right)},\quad (D<h<D+b) \cdots\cdots (39a)$$

$$=\sqrt{\frac{2}{\rho C}fS\frac{t_g}{a}\left(1+K\frac{t_g}{b}\log\frac{10^m}{T}\right)},\quad (h>D+b) \cdots\cdots (39b)$$

where, $\rho=1000/9.8$ kg·sec^2/m^4, D=elevation of the lower frame of the window, d= distance from upper frame of window to the water surface, b=height of window, h= water depth. Some critical lines concerning the window glass breaking are shown in **Figs. 18(a)** and **(b)** for the various kind of window glass dimensions listed in **Table 5.** In these figures, critical lines for the destruction of a wooden house are also drawn. It is found from these figures that, in general, the risk of window glass shattering will be higher than that of wooden house destruction until the water level just reaches the upper frame of a glass. It must be noted, however, window glass is easily broken by drifting objects.

5. Hazard Analysis in the Ogura Basin

5.1 Outline of the Study Area and the Previous Disasters in This Basin

The study area, called 'Ogura basin', is situated in the southern part of Kyoto prefecture, Japan. This area is enclosed by moutains and the banks of two rivers, the Kizu and the Uji, and the total area is about 52 km^2. Recent urbanization accompanied by

increase in population in this area is remarkable. The present density distribution of houses and other structures in this area is shown in **Fig. 19,** classified by the percentile of the total house areas in the 125 m mesh size grid area. Elevation distribution in this area is shown in **Fig. 20.** It can be seen that the urban areas have been developed along the Kintetsu railway, but in recent yaers, residential development has taken place

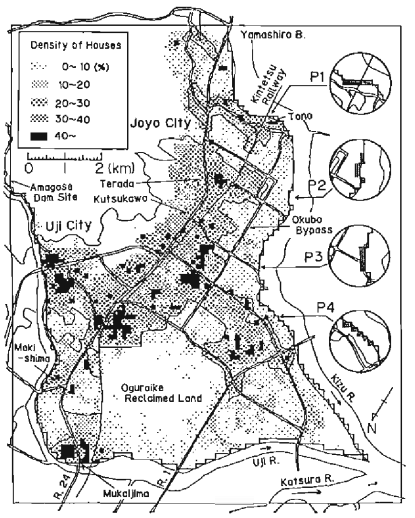

Fig. 19. Distribution of density of houses in the calculation domain.

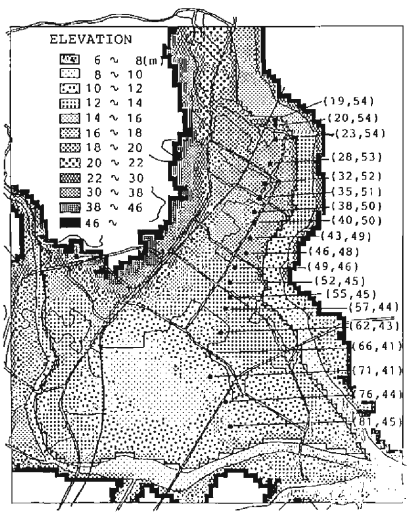

Fig. 20. Distribution of elevation in the study area.

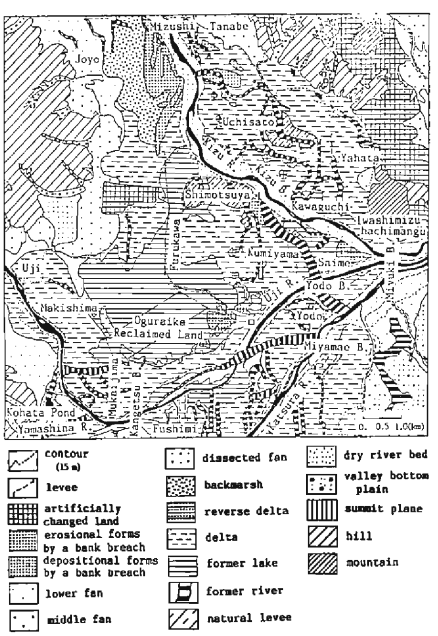

Fig. 21. Classification of the topography in the southern part of the Kyoto basin.

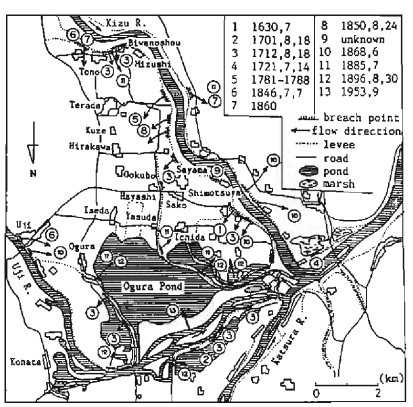

Fig. 22. Previous breach points in the Ogura basin.

even in low lying areas. From a topographical point of view, this area has a cone-shape with reclaimed land that was once Ogura pond situated in the middle of this area. So that, wherever a river bank breach might happen, flood water would flow into this reclaimed land, and the rising water would concentrate in and reform Ogura pond again.

Fig. 21 is a topographic map of the southern part of Kyoto basin[11]. A large part of this basin is formed by the former lake, delta and back marsh of the Kizu river, and many former rivers can be seen. Depositional and erosional forms due to the bank breaches exist near the Mizushi and Shimotsuya districts along the easterly bank of the Kizu river. Especially, in the neighbourhood of the Mizushi district, this configuration extends about 1 km wide and 3 km long. From such topography, it is easy to suppose that this area had experienced large scale disasters due to bank breaches in the past and in reality, as shown in **Fig. 22,** we can see the previous bank breach sites[12]. In the Edo era, floods were recorded 8 times from 1630 to 1850. Especially notable is the flood of 8/18 in 1712, when many bank breaches occurred such as at the Biwanoshou, Kouzuya, Shimada and other districts. A bank breach of the main channel of the Kizu river has not occurred since 1885. For the Uji river, 600 m long bank breach occurred along the south side bank at Daikoku site, due to heavy rainfall accompanied by typhoon 5313 in September, 1953. In the following calculation, we will assume 4 bank breach sites ; these sites are also shown in **Fig. 19** nominated as P1, P2, P3 and P4.

5.2 Conditions of Calculation

The study area, enclosed by the heavy lines in **Fig. 20,** was discretized through a 125 m mesh size grid, $\Delta x = \Delta y = 125$ m, on the topographical maps (1/2500), and split time, Δt, was 2 seconds. We used Manning's roughness coefficients, $n = 0.025$ in river channel and $n = 0.04$ on the protected lowland. The two dimensional numerical simulation method was used both in channel and protected lowland under these conditions. The inflow hydrographs at the Yamashiro bridge into the Kizu river and at the Amagase dam site into the Uji river are shown in **Fig. 23.** The hydrograph of the Kizu river was adopted so as to give the peak stage of the flood in the river, where it

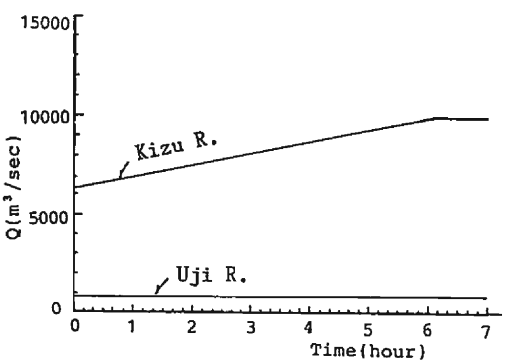

Fig. 23. Test hydrographs at the Yamashiro bridge and the Amagase dam site.

becomes almost the same height as the bank crown. The river water stage was calculated on this basis in an imaginary rectangular cross-section whose bottom coincides with the measured local deepest bottom line. The actual cross-section has a compound shape, and therefore, the cross-section used in the calculation should have been larger than the actual one, which resultantly gave a larger discharge. Thus, the hydrograph used in the calculation has no rational relationship with the design-flood discharge of the river. Provided that the detailed cross-section of the Kizu river are given, the peak discharge of the hydrograph used in the calculation should be less or be nearly equal to the design-flood discharge. By the way, the design-flood discharge of the Kizu river is 6,100 m^3/sec at Haze point near Yamashiro bridge and that of the Uji river is 1,500 m^3/sec at Uji point.

It must be noted here that the object of this study is not to discuss the hazard in detail in this particular basin but to present a general method to estimate the damage cost in an arbitrary basin. Therefore, we haven't paid critical attention to the discrepancy between the hypothetical hydrograph and that of design-flood.

The initial condition of the protected lowland was dry bed and that of the river was made by giving constant discharges of 6,300 m^3/sec and 800 m^3/sec at the inflow point of the Kizu and the Uji river, respectively, and by calculating the water stages under these inflow discharges for 4 hours until the flow reached a steady state. For the downstream boundary condition, we assumed that the river water flows out of the boundary by only the water surface gradient. We neglected the influence of the confluence of the Katsura river downstream, and we did not consider the confluence

Table 6. Test cases for simulation analysis.

CASE	conditions of bank breach	breach point	year
CASE-A	sudden breach	P1	on 1983
-A′	15min required	〃	〃
-B	sudden breach	P2	〃
-B′	15min required	〃	〃
-C	sudden breach	P3	〃
-C′	15min required	〃	〃
-D	sudden breach	P4	〃
-D′	15min required	〃	〃
-E	sudden breach	P1	on 1965
-F	〃	P2	〃
-G	〃	P3	〃
-H	〃	P4	〃
-I	sudden breach & closing 2.5 hr after	P1	on 1983

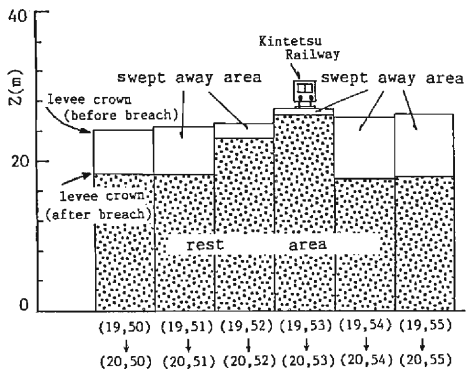

Fig. 24. Example of the scales and elevations for brach point P1 meshes in calculation before and after the bank breach.

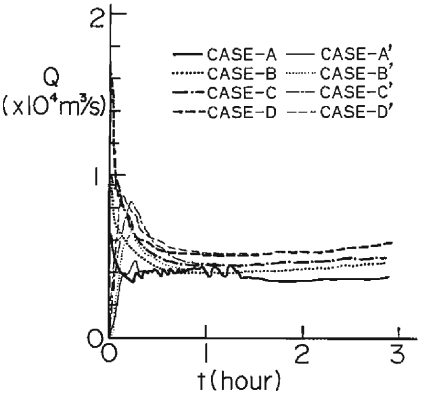

Fig. 25. Outflow discharges of each bank breach point.

of the tributaries and the drainage network systems in this basin. In **Table 6,** the test cases for this simulation analysis are shown.

We examined two cases of bank breach and their causative conditions, first, a bank collapse occurring in an instant and second, one taking 15 minutes for the bank to be breached completely. The width of the bank breach was 6 meshes long which is equal to 750 m, but if these meshes are diagonally located, the width of the bank breach would be larger than 750 m. We also assumed that the levee height after bank breach reduced to that of the inland elevation. **Fig. 24** presents an examble of the width and the elevation of each mesh site P1, before and after the bank breach.

In all cases, if the condition for wooden house removal by flood is satisfied in a certain mesh$(i+1/2, j+1/2)$, we put $\beta_{i+1/2,j+1/2}$ equal to unity to take into account the influence of interference of houses washed into to the surrounding meshes.

5.3 Results of Calculation

The discharge hydrographs at the breach points for every case are shown in **Fig. 25.** In the case of instantaneous break, the maximum discharge from the breach occurred simultaneously with the instant of breach and it was quite a large value. In every case, outflow discharge asymptotically became steady within about an hour. The hydrograph was different in each case, and the reason being that the water level in the channel and the width of the bank breach were different case by case. In the cases where it took 15 minutes for a bank to be breached, peak discharges were lower than those of the instantaneous bank breach cases, and the maximum discharges took place at a rather early stage of the breach. It was found that nearly 50% of the river discharge outflowed from a breach point into the protected lowland in CASE-A and CASE-A′ within about two hours after the bank breach, and in the other cases, more than 50% of the river discharge outflowed there.

Fig. 26 shows the calculated results of the water depth distributions at 4 hours after bank breach in each case. In almost every case, water depth in the Ogura

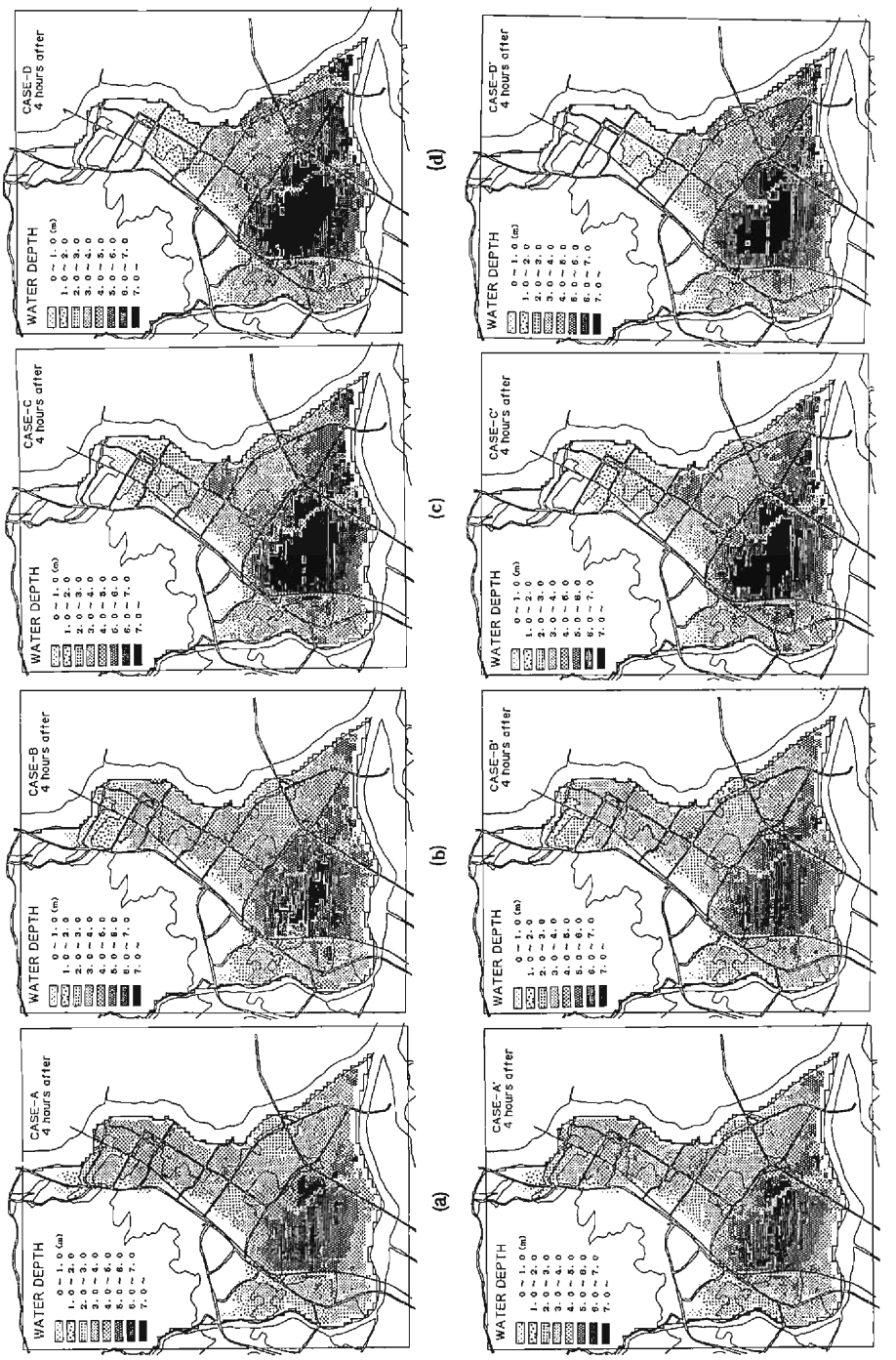

Fig. 26. Calculated results of the water depth distribution at 4 hours after bank breach.

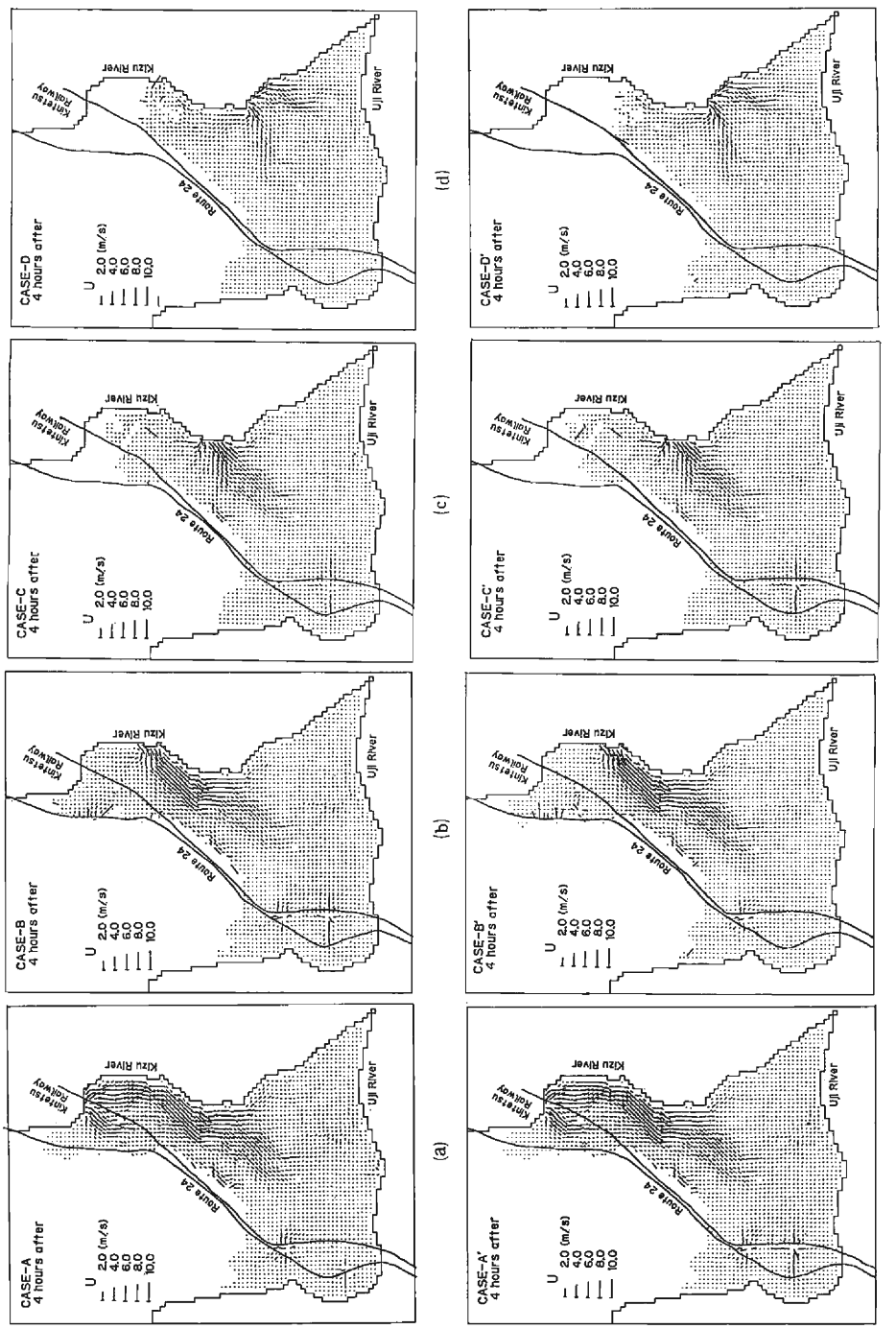

Fig. 27. Calculated results of the flow patterns at 4 hours after bank breach.

reclaimed land was more than 7 m. In CASE-A and CASE-A′, a large part of the Tono and Terada districts were inundated more that 4 m deep, but in the other cases, as the elevation was comparatively high in these districst, they were only slightly or not inundated. These figures show that at 4 hours after bank breach, flooding water had already expanded to the Makishima and the Mukaijima districts overflowing the bank of the Kintetsu railway. In the case where 15 minutes were required until the bank was fully broken, water depth in the Ogura reclaimed land was slightly lower than that in the case of sudden bank breach ; however, there were some areas inundated over 7 m.

The calculated results for flow patterns are shown in **Fig. 27** at 4 hours after bank breach. In every case, the velocity was large near the breach site. In CASEs-C, C′, D and D′, because of the influence of stagnant water in the Ogura reclaimed land, flow rate rapidly decreased some distances from the breach site, and it was extremely low within the Ogura reclaimed land, while in the CASEs-A, A′, B and B′, for the reason that the bed slope was comparatively steep at the southern part of the basin, quite a high velocity was calculated toward the Ogura reclaimed land.

Fig. 28 shows the time variations of the water level at each point shown in **Fig. 20.** From these figures, we were able to estimate the advancing velocity of the forefront. In CASE-A, it was about 4 km/hour near the breach point. The increasing rate of the water depth at the higher elevation area was very large in the early stage but soon became slight, while it was gradual but continued for a longer time in the lower elevation areas.

Fig. 29 shows the maximum degree of damage of wooden houses under the conditions of $M_V=418730$ Nm, $C_D/2=1.064$, $h_c/h=0.732$, $\rho=1000$ kg/m^3 and $B=10$ m. As the critical value of uh is calculated as 7.4 m^2/sec by using these values, the Reynolds number, when we discuss whether a house will swept away, is more than 7.4×10^6. Therefore, experimental results concerning C_D shown in **Fig. 12** can be applid to the range of Reynolds numbers in the actual overland flood flows. The hundred percent of damage degree in the figure corresponds to the critical value of uh for house destruction calculated by eq. (36). Damage degree was classified into 5 ranks, and each rank means the percentile of this critical value. In calculation, h and u were evaluated by using eq. (27) and the following equation, respectively,

$$u=\{(\tilde{M}^{n+2}_{i,j+1/2}+\tilde{M}^{n+2}_{i+1,j+1/2})^2+(\tilde{N}^{n+2}_{i+1/2,j}+\tilde{N}^{n+2}_{i+1/2,j+1})^2\}^{1/2}/(2\tilde{h}^{n+3}_{i+1/2,j+1/2}) \quad \cdots\cdots(40)$$

These figures proved that in the vicinity of the breach site, uh exceeded this critical value and there was scarce difference between instantaneous and 15 minute bank breach. CASEs-A, A′, B and B′ gave large uh values in the area between the Okubo-bypass and east side bank of the Kizu river. A large part of this area is used for agriculture and there are few houses, so that the flooding water is neither interrupted nor contracted to produce large uh values. We were able to understand this situation by referring to **Fig. 27.**

In the Ogura reclaimed land, water depth was very high but the damage degree took relatively small values as the velocity was slow. But if we can consider the effects of buoyancy additionally to the risk of washing away, the degree of damage could be

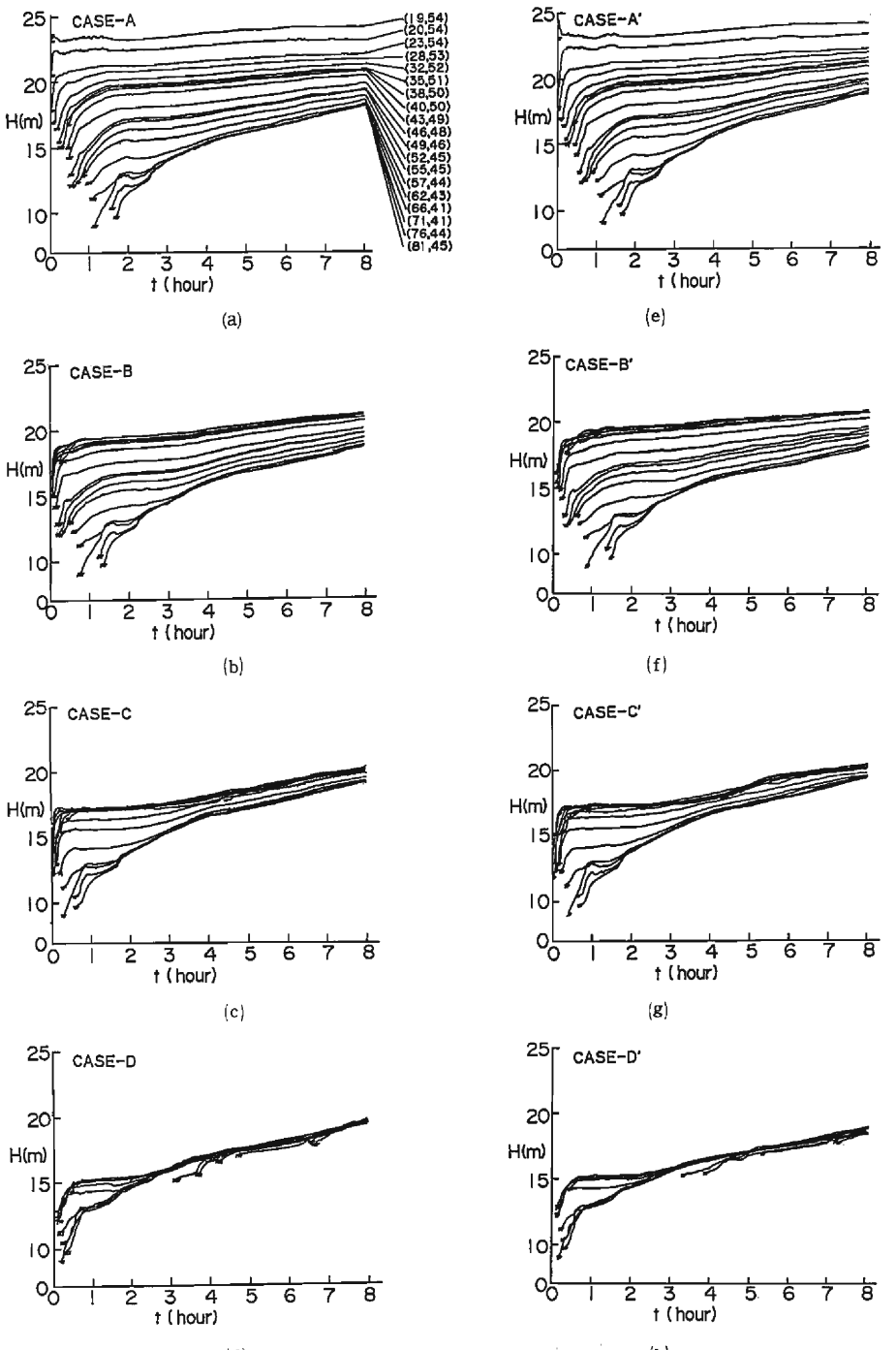

Fig. 28. Time variation of the water level at each point shown in Fig. 20.

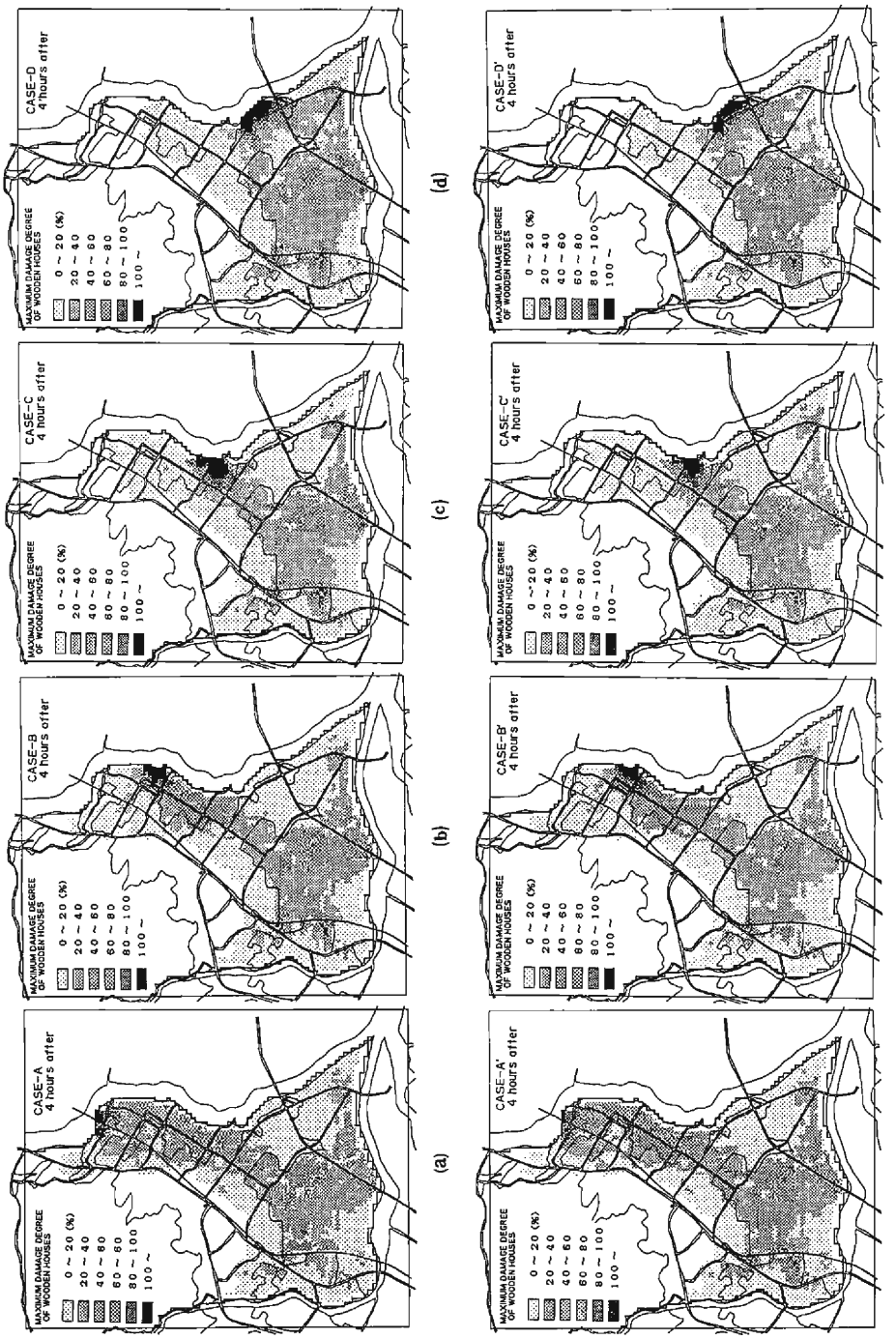

Fig. 29. Calculated results about maximum degree of damage of wooden houses at 4 hours after bank breach.

more.

6. Estimation of the Damage Cost

In order to evaluate the flood hazard risk of a certain basin, it is necessary to quantify the risk. Apart from loss of life, one possible quantifying method is to evaluate the expected value of damage cost to general property (house, household articles and etc., crope, public utilities and so forth). If the mesh data, such as area rates occupied by domiciles, commercial structures, farms, etc. are prepared, we will be able to

Table 7. Damage factor of houses due to floodings

properties \ water depth		below floor	above floor (m)				
			0.0～0.5	0.5～1.0	1.0～2.0	2.0～3.0	3.0～
house	group-A	0.03	0.053	0.072	0.109	0.152	0.220
	-B		0.083	0.126	0.177	0.266	0.344
	-C		0.124	0.210	0.308	0.439	0.572

group-A bed-slope $i<0.001$
-B $0.001<i<0.002$
-C $0.002<i$
(if the water depth is greater than 2.0m above the first floor, damage factor is taken unity for the 45% of the total number of the house)

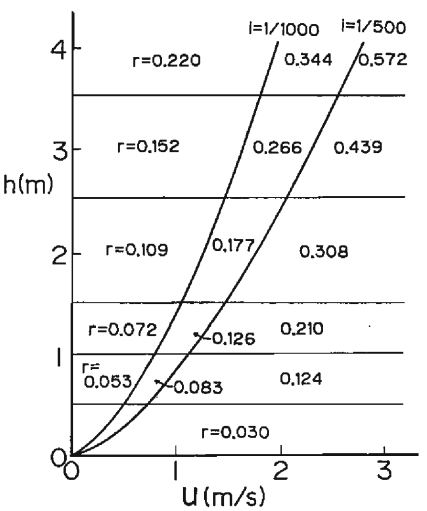

Fig. 30. Relationship between velocity and water depth for the damage factor.

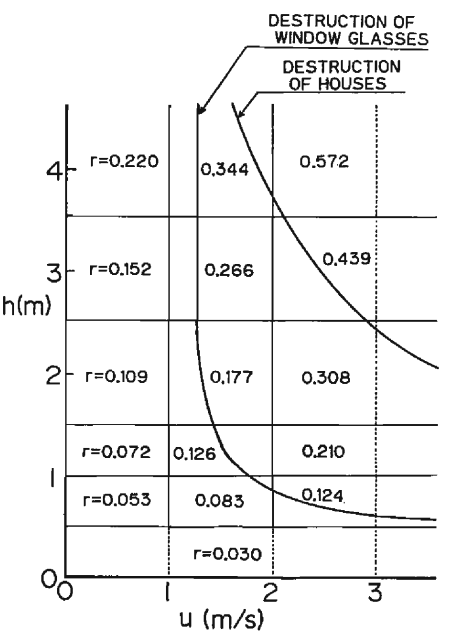

Fig. 31. Modified relationship between velocity and water depth for the damage factor.

estabilish the cost of damage by the numerical simulation method described earlier. In the present study, as the information available was limited to the structure area rate in a mesh, only the house damage was examined. It must be noted here that because the aim of this chapter is focussed on not to quantify the damage of the particular case of Ogura basin, but to discuss the feasibility of the proposed numerical simulation method, discussion taking notice of only house damage should be sufficient for the theoretical purpose.

Table 7 is the Japanese standard[13] to estimate the damage factor r for the house in respect to the various water depths above and below the floor by a flooding. This tabulated standard would be transformed to the graph on the velocity-water depth plane as seen in **Fig. 30,** by using Manning's formula taking the roughness coefficient $n=0.04$. This figure shows that it contains a contradiction, namely, under a constant velocity, lower water depth sometimes can produce higher damage factors than that of greater depth. Therefore, we modified this relationship as shown in **Fig. 31.** Critical lines concerning house and window glass destruction are also presented in this figure. By use of the damage factor related to this velocity and water depth, we estimated the damage index $E_{Fi+1/2,j+1/2}$ in each mesh and total damage index E_T, given by :

$$E_{Fi+1/2,j+1/2}=r_{i+1/2,j+1/2}(1-\beta^2_{i+1/2,j+1/2}) \quad \cdots\cdots(41)$$

$$E_T = \sum_i \sum_j E_{Fi+1/2,j+1/2} \quad \cdots\cdots(42)$$

where, $\beta_{i+1/2,j+1/2}$=flux correction factor given by eq. (24).

Fig. 32 shows the calculated distribution of the damage index E_F for CASEs-A, B, C and D at 4 hours after bank breach. If the water depth was greater than 2.0 m above the first floor, the damage factor was taken as unity for 45% of the total number of the houses as stated in the standard. Naturally, the damage index took large values where the density of houses was high. For each case, the Ogura reclaimed land, the lowest elevation area, had little damage for the reason that there were few houses in this area, but in the surroundings of this area, the number of residences had been increasing, so that a high damage index area existed there. In recent years, buildings have become much denser in the vicinity of point P1, so that, for CASEs-A and A′, E_F's in the vicinity of P1 are of course very high. Whereas, in cases of breach at P2, P3 and P4, E_F's in the vicinity of P1 are small or even zero because the elevation there is comparatively high and inundation would not extend there.

In order to evaluate the influence of urbanization, we calculated the damage under the conditions of 1983 vs. 1965. Moreover, we examined the would be effects of flood fighting efforts to close the breach during flooding.

In **Fig. 33,** time variation of the total damage index E_T are shown. This index in 1983 took 3 and half times larger values than in 1965. We can say this study area has increased its damage potential by urbanization. Wherever the bank breach might occur, the tendency of increase with time of the total damage index was similar. If we couid succeed in closing the breach 2.5 hr after collapse, the total damage index would decrease by about 10 (CASE-I).

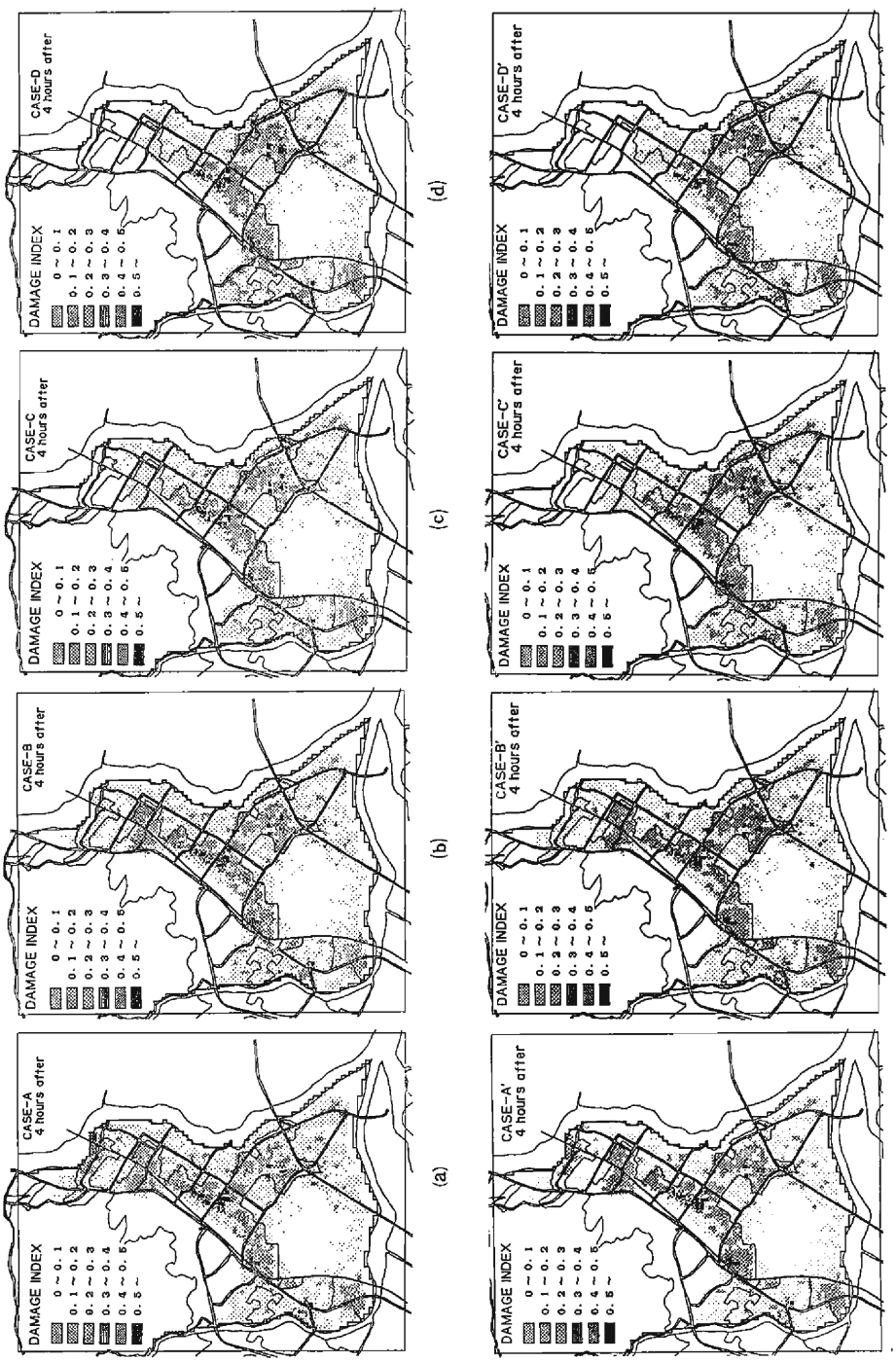

Fig. 32. Calculated results giving the maximum damage index distribution at 4 hours after bank breach.

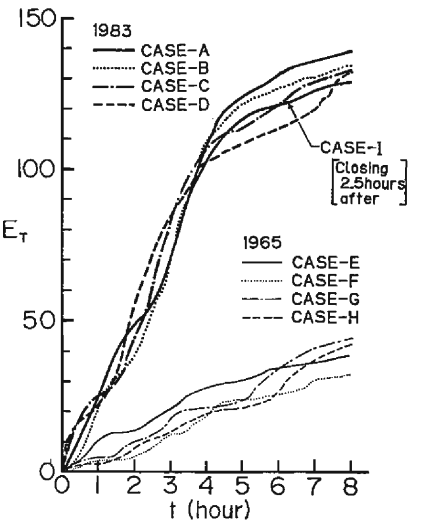

Fig. 33. Time variation in relation to the total maximum damage index.

The total damage cost may be estimated by the following relation :

$$C_T = E_T(\Delta x \Delta y) C_0 / A_0 \quad \cdots\cdots (43)$$

where, C_T=total damage cost, C_0=worth of a house, A_0=area occupied by a house. Supposing that the worth of a house was about 7 million yen and the area of a house is 70 m^2, the total cost of damage is calculated to be about 200 billion yen. Moreover, it was found that the effects of closing the breach, the cost damage would decrease by about 16 billion yen.

If we had considered the damages to crops, public utilities, etc., the influence of drainage system, and the damage due to sedimentation, we would be able to estimate the cost of damage more accurately and reliably.

7. Conclusion

The results obtained in this study are summarized below :

(1) We proposed a simulation method for overland flood flows with consideration of the effects of structures in the flood area.

(2) We examined the applicability of this simulation method by comparing it with experimental laboratory results. Consequently, it was found that the model presented was able to simulate an inundation process accurately.

(3) We proposed criteria which might determine whether the wooden houses would be swept away. Moreover, resistance of window glass against hydrodynamic pressure was examined and it was found that the risk of window glass failure which might result concomitantly to severe damage to the house was higher than that of house destruction.

(4) We applied the simulation method combined with the criteria for house destruc-

tion to the Ogura basin. Under several calculation conditions, we attempted to estimate the hazard risk during inundation.

(5) The feasibility of the damage cost being evaluated by calculating the damage factor in combination with the numerical simulation method was seen. Because the various mesh data on the population, property, etc. can be easily combined with the mesh information of velocity and depth of a flood in the numerical simulation, this method is feasible in risk analysis.

Acknowledgements

We thank Mr. S. Kanou, Mr. T. Nishizaki, Mr. S. Kawanishi and Miss. K. Ishikawa for their help in execution of the experiments and data processing.

The main part of the numerical simulation were performed on FACOM M780 at the Data Processing Center of Kyoto University.

Some part of this study was financially supported by a Grant in Aid of Science Research on Natural Disasters [No. 61025032 organized by the senior author, 1986] from the Japanese Ministry of Education, Culture and Science.

References

1) Takahashi, T., H. Nakagawa and T. Nishizaki: Two Dimensional Numerical Simulation Method to Estimate the Risk of a Flood Hazard Caused by a River Bank Breach, Annuals, Disas. Prev. Res. Inst., Kyoto Univ., No. 29B-2, 1986, pp. 431-450 (in Japanese).
2) Iwasa, Y. and K. Inoue: Flood Invasion Analysis in Flood Plains by Means of Mathematical Simulations, Proc. 21st Symposium on Natural Disas. Sci., 1984, pp. 343-346 (in Japanese).
3) Xanthopoulos, T. and C. Koutitas: Numerical Simulation of a Two Dimensional Flood Wave Propagation due to Dam Failure, Jour. Hydraulic Research, Vol. 14, No. 2, 1976, pp. 321-331.
4) Aida, I.: Numerical Experiments for Inundation of Tsunamis—Susaki and Usa, in Kochi Prefecture—, Bull. Earthq. Res. Inst., Tokyo Univ., Vol. 52, 1977, pp. 441-460 (in Japanese).
5) Nakagawa, H. and T. Takahashi: Study on the Inundation in the Modeled Urban Area due to Bank Breach, Proc. 40th Annual Conf. JSCE, 2, 1985, pp. 113-114 (in Japanese).
6) Goto, C., N. Shuto and T. Sasagawa: Effects of Large Obstacles on Tsunami Inundation, Proc. 25th Japanese Conf. on Hydlaulics, 1981, pp. 125-132 (in Japanese).
7) Kawata, Y. and H. Nakagawa: Flood Disasters in the Misumi River—Flooding and Damages of Houses—, Annuals, Disas, Prev. Res. Inst., Kyoto Univ., No. 27B-2, 1984, pp. 455-470 (in Japanese).
8) Takahashi, T., H. Nakagawa and S. Kanou: Risk Estimation against Washed Away of Wooden Houses by a Flooding, Annuals, Disas. Prev. Res. Inst., Kyoto Univ., No. 28B-2, 1985, pp. 455-470 (in Japanese).
9) Murota, T., T. Arima, H. Okada, M. Sato, K. Saito and K. Mashita: A Full-Scale Test on a Typical Japanese Wooden House Subject to Cyclic Static Lateral Load, Kenchiku Kenkyu Shiryo, Buil. Res. Inst., Ministry of Const., 1981, pp. 1-47 (in Japanese).
10) Ishizaki, H. : Problems in the Design of Window against Wind Pressure, Annuals, Disas. Prev. Res. Inst., Kyoto Univ., No. 19B, 1976, pp. 269-278 (in Japanese).
11) Oya, M.: Materials for the Lecture Titled "Topography and Flooding in Ogura Basin", 8th Seminar for the History of Disaster, Disas. Prev. Res. Inst., Kyoto Univ., 1985.
12) History of the Ogura Pond Reclamation by Drainage, Ogura Pond Soil Amendment Bureau, 1981, pp. 149-160 (in Japanese).
13) Outline of Flood Prevention Economic Survey, River Planning Division of River Bureau, Ministry of Const., 1984, p. 9 (in Japanese).